

Convolutional Prompting for Broad-Domain Retinal Vessel Segmentation

Qijie Wei¹ Weihong Yu^{2,3} Xirong Li^{1,3*}

¹Renmin University of China, China

²Peking Union Medical College Hospital, China

³Beijing Key Laboratory of Fundus Diseases Intelligent Diagnosis & Drug/Device Development and Translation

Abstract—Previous research on retinal vessel segmentation is targeted at a specific image domain, mostly color fundus photography (CFP). In this paper we make a brave attempt to attack a more challenging task of broad-domain retinal vessel segmentation (BD-RVS), which is to develop a *unified* model applicable to varied domains including CFP, SLO, UWF, OCTA and FFA. To that end, we propose *Dual Convolutional Prompting* (DCP) that learns to extract domain-specific features by localized prompting along both position and channel dimensions. DCP is designed as a plug-in module that can effectively turn a R2AU-Net based vessel segmentation network to a unified model, yet without the need of modifying its network structure. For evaluation we build a broad-domain set using five public domain-specific datasets including ROSSA, FIVES, IOSTAR, PRIME-FP20 and VAMPIRE. In order to benchmark BD-RVS on the broad-domain dataset, we re-purpose a number of existing methods originally developed in other contexts, producing eight baseline methods in total. Extensive experiments show the proposed method compares favorably against the baselines for BD-RVS.

Index Terms—Retinal vessel segmentation, Broad-domain, Convolutional prompting

I. INTRODUCTION

Retinal blood vessel characteristics are associated to both ocular and systemic health conditions [1]–[3]. For an accurate analysis of these vascular features, precise retinal vessel segmentation (RVS) in *en face* retinal images is crucial. Moreover, the complexity of our retina requires varied fundus imaging techniques including color fundus photography (CFP), scanning laser ophthalmoscopy (SLO), ultra-widefield fundus imaging (UWF), optical coherence tomography angiography (OCTA), fundus fluorescein angiography (FFA), *etc.* Images produced by a specific imaging technique form a specific *domain*. For better visualization and diagnosis, cross-domain image registration and fusion are needed, for which RVS is often a prerequisite [4]. In such a context, an RVS model that universally works for varied domains will be handy.

Narrow-domain RVS has been extensively studied, mostly on the CFP domain, with improvements in network architectures [5]–[7], training strategies [8]–[11], and both [12]. Furthermore, there are few works on other domains such as UWF [13], [14] and OCTA [15], [16]. Different from these efforts, in this paper we consider a more challenging task of *broad-domain* retinal vessel segmentation (BD-RVS). As

This work was supported by NSFC (62172420) and National High Level Hospital Clinical Research Funding (2022-PUMCH-C-61).

*Corresponding author: Xirong Li (xirong@ruc.edu.cn)

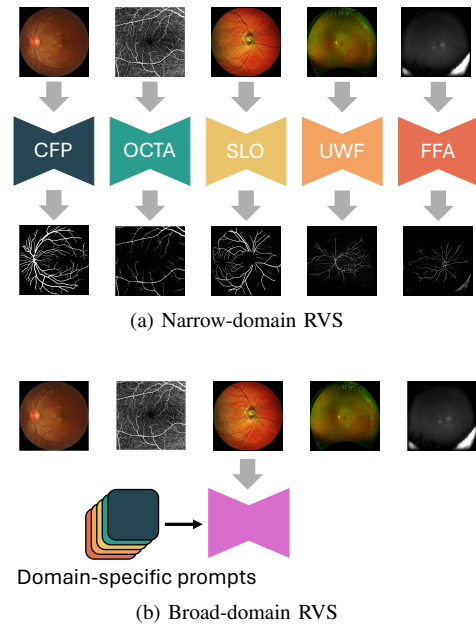


Fig. 1: **Two paradigms for retinal vessel segmentation (RVS)**: (a) narrow-domain and (b) broad-domain. This paper aims for the latter.

shown in Fig. 1, we aim for a *unified* RVS model applicable to five distinct domains.

Developing a model for BD-RVS is nontrivial. Due to the large disparity in their visual appearance, simply training on domain-mixed data is ineffective for learning domain-specific features. Domain adaptation improves a model’s performance on a target domain, yet practically at the cost of performance degeneration on the source domain where the model is originally trained [17]. Prompt learning, originally developed for adapting pre-trained large language models to varied NLP tasks with minimal training data, is gaining popularity for both generic [18], [19] and medical [20] image analysis. For natural image classification, Tsai *et al.* [19] introduce Convolutional Visual Prompt (CVP), which uses a single conv. layer as a prompt applied to the input image. Such a shallow prompt is unlikely to be sufficient to cover the large inter-domain divergence in retinal images. In the context of brain tumor segmentation, Lin *et al.* [20] propose `prompt-DA`, which uses an extra domain classification network to extract

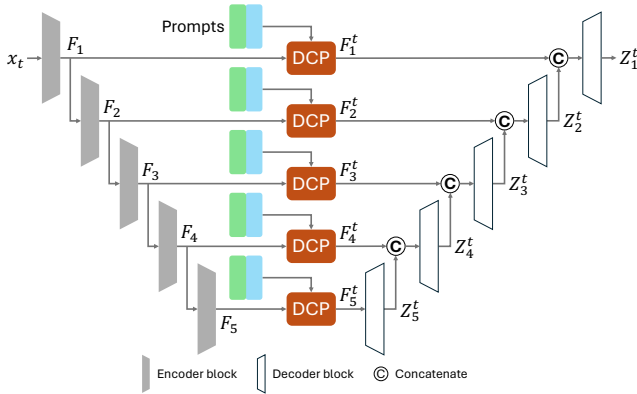


Fig. 2: Our DCP method for broad-domain RVS

domain-related features as a prompt and fuses the prompt with domain-independent features in a holistic manner. Such a fusion strategy might fail to extract local domain-specific features important for segmenting thin vessels and capillaries. Hence, although good performance has been reported on their own tasks, we argue that the current prompt learning methods are suboptimal for BD-RVS.

The main contributions of this paper are as follows:

- To the best of our knowledge, we are the first to attack the challenging task of BD-RVS, developing a unified model that works for five retinal-image domains including CFP, OCTA, SLO, UWF and FFA.
- We propose *dual convolutional prompting* (DCP), extracting domain-specific features by localized prompting in both position and channel dimensions. DCP is designed as a plug-in module such that it can be used with a well establish RVS network without changing the network structure.
- Experiments on a broad-domain set, comprised of five public datasets, show the viability of DCP for BD-RVS. Code is available at <https://github.com/ruc-aimc-lab/dcp>.

II. PROPOSED METHOD

We formalize the BD-RVS task as follows. We assume the availability of labeled training data from T image domains. For each domain $t \in \{1, 2, \dots, T\}$, we have a set of n_t annotated images $\mathcal{N}_t = \{(x_t, y_t)\}$, where x_t indicates a specific image with y_t as its binary vessel mask. The goal of BD-RVS is to train a unified retinal vessel segmentation model based on the multi-domain training data $\mathcal{N}_1 \cup \dots \mathcal{N}_T$. Our method for BD-RVS is to inject domain-specific knowledge and consequently extract domain-specific features via dual convolutional prompting (DCP) into a well established network. In particular, our method works as a plug-in module so that the existing network needs no structural change. In what follows, we describe briefly the overall network in Sec. II-A followed by DCP in Sec. II-B.

A. The Segmentation Network

We adopt R2AU-Net [7] for its good performance on retinal vessel segmentation. R2AU-Net improves the classical

U-Net network [21] by adding attention-enhanced recurrent residual blocks [22], [23]. A common implementation of U-Net (and its variants like R2U-Net [23] and R2AU-Net) uses five convolutional encoders to reduce the input image into an array of progressively downsized feature maps. The feature maps then one-by-one go through five convolutional decoders to generate upsized feature maps. More formally, letting F_i be the output of the i -th encoder and Z_i the output of the i -th decoder, $i = 1, \dots, 5$, the workflow of U-Net can be expressed as

$$\begin{cases} F_i \leftarrow \text{Encoder}_i(F_{i-1}), \\ Z_i \leftarrow \text{Decoder}_i([Z_{i+1}; F_i]), \end{cases} \quad (1)$$

where F_0 is the input image, Z_6 is null, and Z_1 is a probabilistic segmentation output. The input of each decoder is enhanced by recycling the output of the encoder at the same level through a skip connection. As illustrated in Fig. 2, Our DCP module is added to the skip connection, producing a domain-specific feature map F_i^t that has the same shape as F_i . As such, the network structure of R2AU-Net requires no change. Feeding F_i^t into the decoder yields Z_i^t . By executing $\text{Decoder}([Z_{i+1}^t; F_i^t])$, domain-specific decoding is achieved with ease.

B. The Dual Convolutional Prompting Module

In order to extract domain-specific features, we design DCP as follows. Recall that each encoder of the segmentation network outputs an array of feature maps F . Suppose F has C channels, each with a spatial resolution of $H \times W$. Different channels typically capture different visual patterns, whilst feature values at a given spatial position indicate the local presence or absence of the patterns. Hence, jointly prompting along the position and channel dimensions is necessary. Moreover, we are inspired by translation invariance in convolutional neural networks, where the same conv. filter is applied to different positions of a given image or feature map. We thus choose to apply domain-specific prompts in a similar manner. Putting the above thoughts into practice, DCP has three blocks, *i.e.* feature partition, dual prompting, and prompted-feature fusion, see Fig. 3.

Feature Partition. For localized prompting, the feature maps F are partitioned into 8×8 non-overlapped patches, each sized to $C \times h \times w$, $h = \frac{H}{8}$, $w = \frac{W}{8}$. Since the spatial resolution of F varies with the encoders, fixing the number of patches to 64 is computationally convenient. The same prompt tensors will be used for the individual patches.

Position-wise Prompting. Each patch is concatenated with a domain-specific $C \times \Delta h \times w$ prompt along its height dimension ($\Delta h = h$ in this work). For position-wise feature interaction, we shall view the combined features as a sequence of $(h + \Delta h) \times w$ tokens. In order to make Transformer-based feature interaction computationally affordable, we reduce the sequence length by a scale factor of s , achieved by a conv. operation with stride \sqrt{s} . For the five DCP modules from top to bottom shown in Fig. 2, s is set to 64, 16, 4, 1, 1, respectively. The shortened sequence of length $\frac{h + \Delta h}{s}$ is then fed into a standard multi-head self attention (MHSA) block

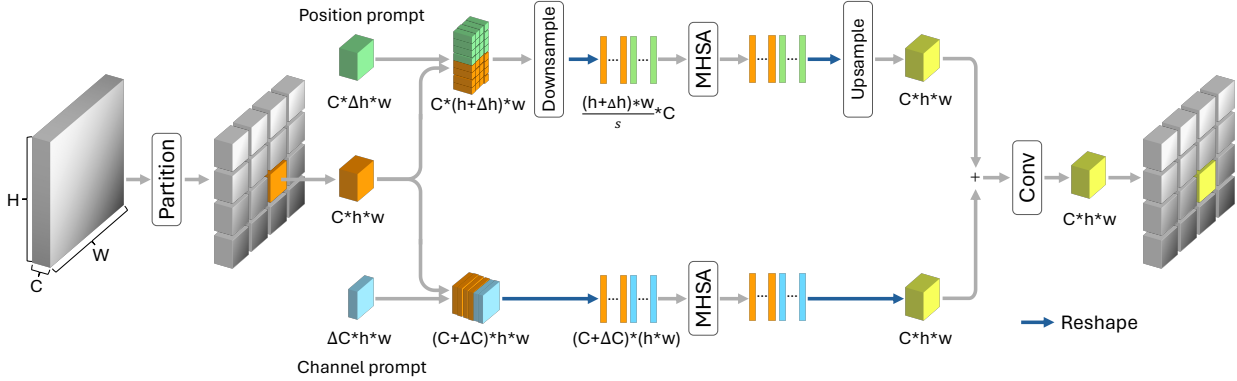


Fig. 3: **Proposed dual convolutional prompting (DCP) module.** Its input is the output feature map of a specific encoder of R2AU-Net. Based on the domain identity of the input image, DCP takes two domain-specific prompt tensors, which interact with the feature maps along the position and channel dimensions, respectively. For *localized* prompting, the feature map is partitioned into smaller (orange) patches. Once trained, the prompts are fixed. Best viewed in color.

[24]. The output sequence, with the prompt tokens removed, goes back to the original-patch size, by reshaping and bilinear-interpolation upsampling.

Channel-wise Prompting. Each patch is concatenated with a domain-specific $\Delta C \times h \times w$ prompt along its channel dimension (here $\Delta C = \frac{C}{4}$). For channel-wise feature interaction, we treat the combined features as a sequence of $C + \Delta C$ tokens and feed the sequence into an MHSA block. The output sequence, with the prompt tokens removed, is reshaped back to the original-patch size.

Prompted-feature Fusion. As shown in Fig. 3, for fusing the dually prompted patches, we simply apply element-wise addition followed by a conv. layer. See Fig. 4 for the effect of DCP on the feature maps.

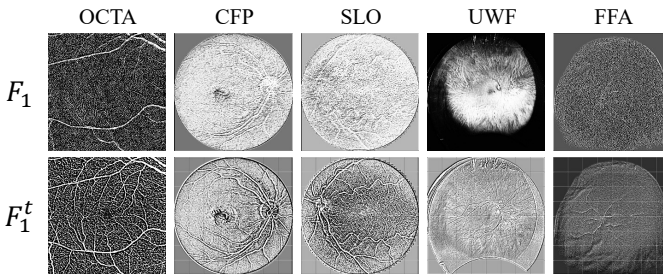


Fig. 4: **Visualization of the input (F_1) and output (F_1^t) of DCP.** For all the five modalities, vessel-related patterns are noticeably enhanced.

III. EXPERIMENTS

A. Experimental Setup

Datasets. To build a broad-domain dataset, we adopt five public datasets, one per modality. That is, ROSSA¹ with 918 OCTA images [15], FIVES² with 800 CFP images [25],

¹<https://github.com/nhjdwyd/OCTA-FRNet>

²https://figshare.com/articles/figure/FIVES_A_Fundus_Image_Dataset_for_AI-based_Vessel_Segmentation/19688169

IOSTAR³ with 30 SLO images [26], PRIME-FP20⁴ with 15 UWF fundus images [14] and VAMPIRE⁵ with 8 FFA images [27]. Each dataset is randomly partitioned into three disjoint subsets for training, validation, and test in a ratio of 7:1:2, respectively. An overview of the data is given in Tab. I.

TABLE I: **Five public datasets used in this study.**

Dataset	Modality	Total	Training	Validation	Test
ROSSA [15]	OCTA	918	642	92	184
FIVES [25]	CFP	800	560	80	160
IOSTAR [26]	SLO	30	21	3	6
PRIME-FP20 [14]	UWF	15	10	2	3
VAMPIRE [27]	FFA	8	5	1	2

Baseline Methods. For a comprehensive comparison, we consider the following eight baseline methods:

- **Narrow-domain:** Five R2AU-Nets, separately trained per domain.
- **Narrow-domain-FT:** First training R2AU-Net on FIVES, *i.e.* viewing CFP as the source domain, and then fine-tuning the model separately for each of the other four domains.
- **Broad-domain:** One R2AU-Net trained on the joint five-domain training set.
- **prompt-DA** [20]. Re-purposing prompt-DA for the BDRVS task, where CFP is treated as the source domain and the other four domains are regarded as the target domains.
- **prompt-SDA.** Note that prompt-DA treats target-domain training samples *unlabeled*. For a more fair comparison, we extend prompt-DA to supervised domain adaptation [28] to learn from the labeled target-domain data.
- **MedSAM** [29]: MedSAM, a state-of-the-art Vision Transformer based medical image segmentation network, fine-tuned on our broad-domain training data.
- **MedSAM-VPT.** Adapting MedSAM by visual prompt tuning

³<https://www.retinacheck.org/download-iostar-retinal-vessel-segmentation-dataset>

⁴<https://iee-dataport.org/open-access/prime-fp20-ultra-widefield-fundus-photography-vessel-segmentation-dataset>

⁵<https://vampire.computing.dundee.ac.uk/vesselseg.html>

(VPT) [18].

- CVP [19]: Prepending a domain-specific 3×3 conv. layer to the first encoder block of R2AU-Net.

Implementation Details. For a fair comparison, all experiments are implemented as follows, unless otherwise specified. The segmentation network is R2AU-Net [7], with its encoder replaced by a pruned [30] version of EfficientNet-B3 [31]. All images are resized to 512×512 . Subject to our computing power (4 NVIDIA RTX 3090 GPUs), a mini batch has 5 images, one per domain. The network is trained to minimize the mean of the BCE and Dice losses. The optimizer is SGD with initial learning rate of $1e-3$, momentum of 0.95 and weight decay of $1e-4$. Learning rate is adjusted according to cosine annealing strategy [32]. Validation is performed every epoch. Early stop occurs if there is no increase in performance within 10 successive validations. PyTorch 1.13.1 is used.

Performance Metrics. We primarily report pixel-level average precision (AP), more discriminative than Area under the ROC Curve (AUC) score.

TABLE II: **SOTA for BD-RVS.** Methods sorted in ascending order by their mean AP on the five test sets. Two naive baselines, *i.e.* Narrow-domain with five domain-specific R2AU-Nets and Broad-domain with one R2AU-Net, are marked out in color. Compared with the best-performing baseline (prompt-SDA), DCP is smaller and better.

Method	Params(M)	Mean	ROSSA	FIVES	IOSTAR	PRIME-FP20	VAMPIRE
prompt-DA	16.9	0.3879	0.0553	0.8698	0.8071	0.1649	0.0425
MedSAM-VPT	91.7	0.5621	0.8042	0.7804	0.7528	0.1951	0.2779
MedSAM	91.3	0.5692	0.8059	0.7923	0.7597	0.2041	0.2838
Narrow-domain	42.7	0.6670	0.8561	0.8867	0.8578	0.3720	0.3623
Broad-domain	8.5	0.6717	0.8386	0.8847	0.8559	0.4145	0.3646
CVP	8.5	0.6764	0.8417	0.8614	0.8362	0.3926	0.4502
Narrow-domain-FT	42.7	0.6790	0.8500	0.8867	0.8568	0.3916	0.4099
prompt-SDA	16.9	0.6820	0.8452	0.8834	0.8466	0.4174	0.4175
Proposed DCP	12.5	0.7037	0.8587	0.8928	0.8598	0.4298	0.4776

B. Comparison with SOTA

As shown in Tab. II, the Broad-domain method, despite its simplicity, is ranked at 4/8 among the eight baselines. In particular, it outperforms Narrow-domain on PRIME-FP20 and VAMPIRE, both of which have relatively limited training data. This result suggests that learning from the domain-mixed data is beneficial for the resource-limited domains. This is further confirmed by the better performance of Narrow-domain-FT against Broad-domain on VAMPIRE, obtained at the cost of using multiple models. Compared with the best-performing baseline, *i.e.* prompt-SDA, the proposed DCP is more accurate (0.7037 vs. 0.6820 in AP), yet smaller (12.5M vs. 16.9M in parameters).

In addition, we report the AUC scores in Tab. III. The AUC-based ranking of the different methods is largely consistent with its AP counterpart, except that CVP becomes the best baseline. Our DCP again surpasses the baselines. Some qualitative results are shown in Fig. 5.

C. Ablation study

Tab. IV shows the performance of DCP with varied setups. Removing feature partition / position-wise (pos.) prompting /

TABLE III: **Performance measured by AUC.**

Method	Mean	ROSSA	FIVES	IOSTAR	PRIME-FP20	VAMPIRE
prompt-DA	0.8167	0.4783	0.9782	0.9784	0.8769	0.7717
MedSAM-VPT	0.9438	0.9845	0.9643	0.9644	0.8876	0.9183
MedSAM	0.9451	0.9849	0.9675	0.9666	0.8897	0.9166
Narrow-domain	0.9537	0.9886	0.9837	0.9791	0.9204	0.8968
Broad-domain	0.9664	0.9873	0.9838	0.9857	0.9408	0.9345
Narrow-domain-FT	0.9664	0.9886	0.9837	0.9820	0.9284	0.9492
prompt-SDA	0.9680	0.9873	0.9823	0.9825	0.9437	0.9444
CVP	0.9689	0.9873	0.9804	0.9823	0.9422	0.9521
Proposed DCP	0.9739	0.9887	0.9862	0.9862	0.9537	0.9549

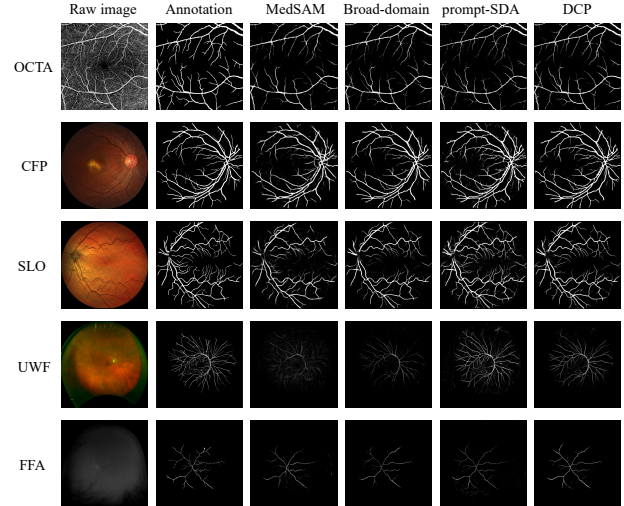


Fig. 5: **Qualitative results.** The efficacy of DCP is primarily manifested in segmenting capillaries. Best viewed digitally.

channel-wise (cha.) prompting consistently results in performance loss. The necessity of these component is thus justified. We also check if similar improvement can be obtained by adding MHSA for position-wise / channel-wise feature interaction *without* using any prompt, see “w/o prompt” in Tab. IV. Its lower performance than “Full” verifies the importance of the prompts.

TABLE IV: **Ablation study.** The performance gap of not using a specific component to the full setup reflects the importance of that component. Metric: AP.

Setup	Params(M)	Mean	ROSSA	FIVES	IOSTAR	PRIME-FP20	VAMPIRE
w/o partition	16.3	0.6781(↓3.6%)	0.8480	0.8839	0.8434	0.4155	0.3997
w/o prompt	12.2	0.6833(↓2.9%)	0.8554	0.8775	0.8527	0.4066	0.4241
w/o pos. prompting	9.1	0.6896(↓2.0%)	0.8394	0.8908	0.8489	0.4205	0.4483
w/o cha. prompting	10.8	0.6915(↓1.7%)	0.8610	0.8828	0.8520	0.4041	0.4577
Full	12.5	0.7037	0.8587	0.8928	0.8598	0.4298	0.4776

IV. CONCLUSIONS

For broad-domain retinal vessel segmentation (BD-RVS), we propose dual convolutional prompting (DCP), a plug-in module effectively turning an R2AU-Net based vessel segmentation network to a unified model that works for CFP, OCTA, SLO, UWF and FFA. Experiments on a broad-domain dataset verifies the effectiveness of the proposed method. Both position-wise and channel-wise prompting are useful. Localized prompting also matters. We believe our study of BD-RVS has opened new opportunities for the long-studied RVS problem.

REFERENCES

- [1] M. Fraz, A. R. Rudnicka, C. G. Owen, D. Strachan, and S. A. Barman, "Automated arteriole and venule recognition in retinal images using ensemble classification," in *VISAPP*, 2014.
- [2] R.-Q. Li, G.-B. Bian, X.-H. Zhou, X. Xie, Z.-L. Ni, Y.-J. Zhou, Y. Wang, and Z. Hou, "Vessel width estimation via convolutional regression," in *MICCAI*, 2021.
- [3] P. Su, Y. Zhao, T. Chen, J. Xie, Y. Zhao, H. Qi, Y. Zheng, and J. Liu, "Exploiting reliability-guided aggregation for the assessment of curvilinear structure tortuosity," in *MICCAI*, 2019.
- [4] J. Zhang, Y. Wang, J. Dai, M. Cavichini, D.-U. G. Bartsch, W. R. Freeman, T. Q. Nguyen, and C. An, "Two-step registration on multimodal retinal images via deep neural networks," *IEEE Transactions on Image Processing*, vol. 31, pp. 823–838, 2021.
- [5] J. Lin, X. Huang, H. Zhou, Y. Wang, and Q. Zhang, "Stimulus-guided adaptive transformer network for retinal blood vessel segmentation in fundus images," *Medical Image Analysis*, vol. 89, p. 102929, 2023.
- [6] C. Wang, R. Xu, S. Xu, W. Meng, and X. Zhang, "DA-Net: Dual branch transformer and adaptive strip upsampling for retinal vessels segmentation," in *MICCAI*, 2022.
- [7] Q. Zuo, S. Chen, and Z. Wang, "R2AU-Net: Attention recurrent residual convolutional neural network for multimodal medical image segmentation," *Security and Communication Networks*, vol. 2021, pp. 1–10, 2021.
- [8] L. Li, M. Verma, Y. Nakashima, H. Nagahara, and R. Kawasaki, "IterNet: Retinal image segmentation utilizing structural redundancy in vessel networks," in *WACV*, 2020.
- [9] Y. Tan, K.-F. Yang, S.-X. Zhao, and Y.-J. Li, "Retinal vessel segmentation with skeletal prior and contrastive loss," *IEEE Transactions on Medical Imaging*, vol. 41, no. 9, pp. 2238–2251, 2022.
- [10] R. Xu, J. Zhao, X. Ye, P. Wu, Z. Wang, H. Li, and Y.-W. Chen, "Local-region and cross-dataset contrastive learning for retinal vessel segmentation," in *MICCAI*, 2022.
- [11] Y. Zhou, H. Yu, and H. Shi, "Study group learning: Improving retinal vessel segmentation trained with noisy labels," in *MICCAI*, 2021.
- [12] W. Liu, H. Yang, T. Tian, Z. Cao, X. Pan, W. Xu, Y. Jin, and F. Gao, "Full-resolution network and dual-threshold iteration for retinal vessel and coronary angiograph segmentation," *IEEE Journal of Biomedical and Health Informatics*, vol. 26, no. 9, pp. 4623–4634, 2022.
- [13] E. Pellegrini, G. Robertson, T. MacGillivray, J. van Hemert, G. Houston, and E. Trucco, "A graph cut approach to artery/vein classification in ultra-widefield scanning laser ophthalmoscopy," *IEEE Transactions on Medical Imaging*, vol. 37, no. 2, pp. 516–526, 2018.
- [14] L. Ding, A. E. Kuriyan, R. S. Ramchandran, C. C. Wykoff, and G. Sharma, "Weakly-supervised vessel detection in ultra-widefield fundus photography via iterative multi-modal registration and learning," *IEEE Transactions on Medical Imaging*, vol. 40, no. 10, pp. 2748–2758, 2020.
- [15] H. Ning, C. Wang, X. Chen, and S. Li, "An accurate and efficient neural network for OCTA vessel segmentation and a new dataset," in *ICASSP*, 2024.
- [16] D. Hu, C. Cui, H. Li, K. E. Larson, Y. K. Tao, and I. Oguz, "LIFE: A generalizable autoidactic pipeline for 3D OCT-A vessel segmentation," in *MICCAI*, 2021.
- [17] J. Wang, K. Tian, D. Ding, G. Yang, and X. Li, "Unsupervised domain expansion for visual categorization," *ACM Transactions on Multimedia Computing, Communications, and Applications*, vol. 17, no. 4, pp. 1–24, 2021.
- [18] M. Jia, L. Tang, B.-C. Chen, C. Cardie, S. Belongie, B. Hariharan, and S.-N. Lim, "Visual prompt tuning," in *ECCV*, 2022.
- [19] Y.-Y. Tsai, C. Mao, and J. Yang, "Convolutional visual prompt for robust visual perception," in *NeurIPS*, 2023.
- [20] Y. Lin, D. Nie, Y. Liu, M. Yang, D. Zhang, and X. Wen, "Multi-target domain adaptation with prompt learning for medical image segmentation," in *MICCAI*, 2023.
- [21] O. Ronneberger, P. Fischer, and T. Brox, "U-Net: Convolutional networks for biomedical image segmentation," in *MICCAI*, 2015.
- [22] O. Oktay, J. Schlemper, L. Le Folgoc, M. Lee, M. Heinrich, K. Misawa, K. Mori, S. McDonagh, N. Y. Hammerla, B. Kainz, B. Glocker, and D. Rueckert, "Attention U-Net: Learning where to look for the pancreas," in *MIDL*, 2018.
- [23] M. Z. Alom, C. Yakopcic, M. Hasan, T. M. Taha, and V. K. Asari, "Recurrent residual U-Net for medical image segmentation," *Journal of Medical Imaging*, vol. 6, no. 1, pp. 014 006–014 006, 2019.
- [24] A. Vaswani, N. Shazeer, N. Parmar, J. Uszkoreit, L. Jones, A. N. Gomez, L. Kaiser, and I. Polosukhin, "Attention is all you need," *NeurIPS*, 2017.
- [25] K. Jin, X. Huang, J. Zhou, Y. Li, Y. Yan, Y. Sun, Q. Zhang, Y. Wang, and J. Ye, "FIVES: A fundus image dataset for artificial intelligence based vessel segmentation," *Scientific Data*, vol. 9, no. 1, p. 475, 2022.
- [26] S. Abbasi-Sureshjani, I. Smit-Ockeloen, J. Zhang, and B. Ter Haar Romeny, "Biologically-inspired supervised vasculature segmentation in slo retinal fundus images," in *ICIAR*, 2015.
- [27] A. Perez-Rovira, K. Zutis, J. P. Hubschman, and E. Trucco, "Improving vessel segmentation in ultra-wide field-of-view retinal fluorescein angiograms," in *EMBC*, 2011.
- [28] Q. Wei, J. Yang, B. Wang, J. Wang, J. Zhao, X. Zhao, S. Yang, N. Manivannan, Y. Chen, D. Ding, J. Zhou, and X. Li, "Supervised domain adaptation for recognizing retinal diseases from wide-field fundus images," in *BIBM*, 2023.
- [29] J. Ma, Y. He, F. Li, L. Han, C. You, and B. Wang, "Segment anything in medical images," *Nature Communications*, vol. 15, no. 1, p. 654, 2024.
- [30] Y. Aflalo, A. Noy, M. Lin, I. Friedman, and L. Zelnik, "Knapsack pruning with inner distillation," *arXiv preprint arXiv:2002.08258*, 2020.
- [31] M. Tan and Q. Le, "EfficientNet: Rethinking model scaling for convolutional neural networks," in *ICML*, 2019.
- [32] I. Loshchilov and F. Hutter, "SGDR: Stochastic gradient descent with warm restarts," in *ICLR*, 2016.